ACS EARTH AND SPACE CHEMISTRY

http://pubs.acs.org/journal/aesccq

Article

Nanoanalytical Identification of Siderite Dissolution-Coupled Pb Removal Mechanisms from Oxic and Anoxic Aqueous Solutions

Lisa C. Füllenbach,* Jeffrey Paulo H. Perez, Helen M. Freeman, Andrew N. Thomas, Sathish Mayanna, Julia E. Parker, Jörg Göttlicher, Ralph Steininger, Jörg Radnik, Liane G. Benning, and Eric H. Oelkers*

Cite This: https://dx.doi.org/10.1021/acsearthspacechem.0c00180 Read Online

ACCESS | Metrics & More | Article Recommendations | Supporting Information

ABSTRACT: Lead(II) is a toxic pollutant often found in metal-contaminated soils and wastewaters. In acidic aqueous environments, Pb(II) is highly mobile. Chemical treatment strategies of such systems therefore often include neutralization agents and metal sorbents. Since metal solubility and the retention potential of sorbents depend on the redox state of the aqueous system, we tested the efficiency of the naturally occurring redox-sensitive ferrous iron carbonate mineral siderite to remove Pb(II) from acidic aqueous solutions in batch experiments under oxic and anoxic conditions over a total of 1008 h. Siderite dissolution led to an increase in reactive solution pH from 3 to 5.3 and 6.9, while 90 and 100% of the initial aqueous Pb(II) (0.48×10^{-3} mol kg^{-1}) were removed from the oxic and anoxic systems, respectively. Scanning and transmission electron microscopy, combined with X-ray absorption and photoelectron spectroscopy, indicated that under oxic conditions, Pb(II) was consumed by cerussite precipitation and inner-sphere surface complexation to secondary goethite. Under anoxic conditions, Pb(II) was removed by the rapid precipitation of cerussite. This efficient siderite dissolution-coupled sequestration of Pb(II) into more stable solid phases demonstrates this potential method for contaminated water treatment regardless of the redox environment.

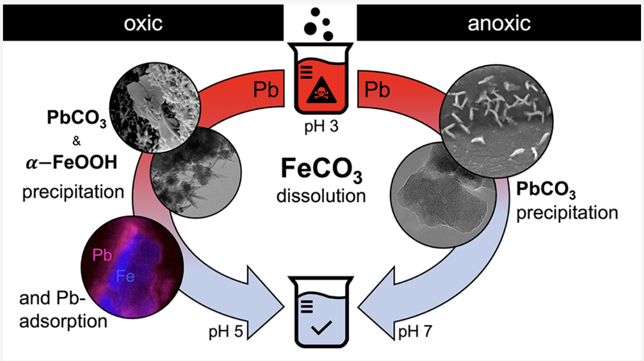

KEYWORDS: *siderite, XANES-mapping, EXAFS, lead carbonate, iron oxyhydroxides, adsorption, wastewater treatment*

1. INTRODUCTION

Human use of land and natural resources often leads to surface and groundwater pollution. Divalent lead (Pb(II)) is one of the most toxic and common contaminants introduced to soils and (sub)surface waterbodies from mine tailings,[1,2] waste disposal and landfills,[3−5] and industrial activities,[6] where concentrations can reach up to several thousand mg of Pb(II) per kg of contaminated soils or sediments.[7−9] Studies of lead removal from aqueous solutions have been mainly focused on chemical sorption under oxic and controlled pH conditions to various substrates including aluminum oxides,[10,11] clays,[12] soils,[13,14] calcite,[15−17] and ferric iron (oxyhydr)oxides such as goethite.[18−20] Contaminated environments such as stream sediments,[21] floodplain soils,[7,8] and tailing dam sites,[9] which are in consistent contact with water, are highly susceptible to redox changes resulting from periodic (*e.g.*, tidal) or seasonal (*e.g.*, heavy rainfall) fluctuations. As the redox state of a polluted aqueous system directly affects the pH and determines the solubility of many metals and sorbents,[21−23] it is necessary to understand the redox state of the system to accurately predict both metal retention and release. Although acidity of wastewaters, as in acid mine drainage,[24] is commonly overcome by the addition of alkaline, often carbonate, materials,[25,26] the issue of potential redox fluctuations causing metal release in contaminated waterbodies remains a challenge.

The redox-sensitive ferrous carbonate siderite ($FeCO_3$) is a potential candidate material for redox-dependent metal remediation. Several studies have investigated siderite as a reductive sorbent for redox sensitive metal(loid)s such as Cr,[27−29] As,[30,31] and Hg.[32] Under controlled pH and redox conditions, these metal(loid)s were reduced and adsorbed to either the siderite surface or, due to coupled redox reactions, to secondary ferric (oxyhydr)oxides. Little attention has been drawn to illuminate the complete reaction pathway between siderite and contaminants over time, where siderite can act as both a dissolution-induced neutralizer and a sorbent under either redox conditions. Siderite is highly soluble in acidic aqueous solutions,[33] and its dissolution leads to aqueous phase neutralization through bicarbonate production. Under oxic

Received: July 7, 2020
Revised: September 22, 2020
Accepted: October 5, 2020

conditions, the release and oxidation of Fe(II) from dissolving siderite result in the precipitation of Fe(III) (oxyhydr)oxides.[34] During dissolution under reduced conditions, iron oxidation is suppressed, and aqueous metals can interact with the siderite surfaces and its dissolution products.

To test whether siderite reactivity in acidic aqueous systems is also sufficient to remove less redox-sensitive metals such as Pb in either redox environments over time and to better understand the mechanisms involved, we have monitored natural siderite dissolution, pH, and metal concentrations in initially acidic Pb(II)-bearing aqueous solutions under oxic and anoxic conditions. We used scanning and transmission electron microscopy (SEM and TEM) to investigate the siderite—precipitate interface and the reaction products. Complimentary X-ray absorption and photoelectron spectroscopic (XAS and XPS) analyses, including high-resolution elemental X-ray fluorescence (XRF) and absorption spectroscopic mapping, allowed localization and determination of Fe(II/III) and Pb(II) speciation and bonding environments. Data acquired from this set of analyses contributes to the evaluation of the metal retention efficiency of siderite as a potential low-cost *in situ* remediation material.

2. MATERIALS AND METHODS

2.1. Materials. Natural macrocrystalline siderite from Peyrebrune Quarry, France,[33] was ground in an agate mortar and sieved to a <63 μm size fraction. The siderite powder was cleaned by repeated rinsing with ethanol after ultrasonication; its surface area was 9.95 m^2 g^{-1}, as determined by BET multipoint krypton adsorption (Quantachrome Autosorb-1MP). Powder X-ray diffraction (XRD; PANalytical X'Pert) confirmed the purity of the cleaned siderite powder (>98%) with minor amounts of fluorite, quartz, and traces of calcite and hematite impurities. Inductively coupled plasma optical emission spectroscopy (ICP—OES; Varian 720ES) of the siderite powder revealed contents of 2.43 wt % Mn, 1.27 wt % Ca, and 0.34 wt % Mg, which are likely structural impurities in siderite and minor calcite. Minor and trace contents of 0.74 wt % S, 0.13 wt % K, 0.02 wt % Na, 0.02 wt % Si, 37.3 ppm Cu, and 24.5 ppm Cr also detected in the ground material are likely contributions from mineral impurities (*e.g.*, quartz and trace sulfides).

2.2. Batch Experiments. All chemicals used in the experiments were of reagent or analytical grade from Honeywell Fluka and VWR and used as received. All aqueous stock solutions were prepared using ultrapure deionized water (Milli-Q, resistivity ~ 18 MΩ cm). The aqueous solutions used in the oxic experiments were prepared under ambient laboratory conditions, whereas those used in the anoxic experiments were prepared inside a CO_2-free anaerobic chamber (97% N_2, 3% H_2; COY Laboratory Products Inc.) using de-oxygenated deionized water that was sparged with argon at ~90 °C for at least 4 h prior to the experiments. For both the oxic and anoxic experiments, the pH of all starting solutions was adjusted to 3.0 ± 0.1 by adding 15.5 M HNO_3 and 2.5 M NaOH, and the ionic strength was adjusted to 2−5 $\times 10^{-3}$ mol kg^{-1} by adding 0.1 M $NaNO_3$. For all lead-bearing solutions, 0.48×10^{-3} mol kg^{-1} lead(II) nitrate ($Pb(NO_3)_2$) was dissolved into deionized water prior to ionic strength and pH adjustment. The concentrations of lead used in the experiments are based on average concentrations reported in contaminated environments.[6−9]

All oxic and anoxic experiments were performed in duplicate in batch reactors that were continuously mixed in a rotary mixer. A list of all experimental details is provided in Table S1. For each experiment, based on preliminary experiments (not shown) and studies using siderite as a metal sorbent,[27,29,30] 6 g L^{-1} siderite was reacted with the oxic and anoxic acidic Pb(II)-bearing aqueous solutions. Control experiments in the absence of Pb were also conducted following the same procedures (Figure S1). To allow the analysis of the fluid and the solid phases at various stages of the siderite dissolution reaction, a series of 15 distinct single short-term batch experiments were performed and ended at different times. The experiments in these series ran for 0.5, 1, 2, 3, 6, 12, 20, 28, 36, 48, 60, 72, 96, 144, and 240 h. Additional long-term (LT) experiments were run for a total of 1008 h; during these experiments, fluid aliquots were collected every 168 h. Sampling of liquid aliquots from the oxic experiment was conducted within minutes to avoid equilibration of the reactive fluid with atmospheric CO_2. Final solids and fluids from all experiments were separated for analysis by vacuum filtration using 0.2 μm nylon filters. To avoid potential iron oxidation and to ensure all iron remained dissolved in the filtrates, aliquots were immediately acidified after sampling. The collected solid residues were kept dry or in ethanol at ambient conditions, in the case of the anoxic samples in the anaerobic chamber, to prevent further phase transformation.

The elemental concentrations of all 214 collected fluid samples were measured using ICP—OES (Varian 720ES/Agilent Technologies 5110); the average relative standard deviation (RSD) of the analyses ranged from 0.3 to 1.2% (Table S2). Final liquid samples with Pb concentrations below the detection limit of the ICP—OES were remeasured using the more sensitive inductively coupled plasma mass spectrometer (Bruker 90); analyses were within an accuracy of 0.57% RSD. To determine the oxidation of dissolved Fe^{2+} to Fe^{3+} in the reacted aqueous solutions, Fe speciation was measured by the colorimetric ferrozine method[35] using a segmented flow analysis device (SFA; SEAL AutoAnalyzer 3HR) equipped with a digital colorimeter. The average RSD of these measurements ranged between 0.34 and 0.35%. Comparison of the total iron concentrations determined using SFA (Fe^{total}_{SFA}) to those obtained by ICP—OES (Fe^{total}_{OES}) revealed that $Fe^{total}_{SFA} \approx Fe^{total}_{OES}$, whereupon Fe^{total}_{OES} is a close approximation of the Fe^{2+} released during siderite dissolution (Figure S2).

2.3. Solid-Phase Characterization. Initial and reacted siderite and selected secondary solid reaction products were imaged and analyzed using a ZEISS Ultra Plus Gemini field-emission scanning electron microscope equipped with an In-lens secondary electron and UltraDry SDD energy dispersive X-ray (EDX) detectors. Solids collected from anoxic experiments were mounted onto SEM stubs inside the anaerobic chamber and transported to the SEM facility using an anaerobic jar to avoid sample oxidation.

Bulk mineral structure analyses were performed with a high resolution PANalytical X'pert PRO MPD diffractometer equipped with a Co anode X-ray tube (λ = 1.789 Å), a Ge incident beam monochromator, and an X'celerator detector. Repeated measurements of anoxic samples stored under dry ambient laboratory conditions for 19 h and 5 weeks verified the long term stability of siderite and secondary phases.

High resolution morphological and structural analyses were performed with a FEI Tecnai G2 F20 X-Twin transmission

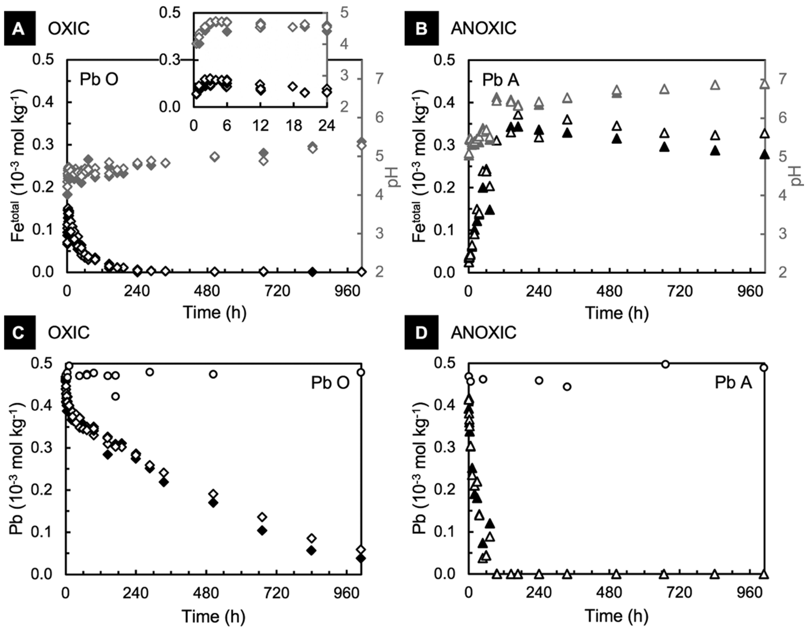

Figure 1. Total metal concentrations (black symbols) and pH (grey symbols) shown as a function of time. Fe^{total} and pH during siderite dissolution in the presence of Pb(II) under oxic (A; diamonds) and anoxic conditions (B; triangles); corresponding Pb(II) concentrations are given in (C,D), respectively (circles = control solutions). Error bars are smaller than the symbols. Standard error of the pH probe is ±0.01 and RSD % (ICP−OES) is 0.29 to 1.23%. Shown are data from all Pb(II)-bearing experiments (Table S1). For clarity, Fe^{total} concentrations and pH measured during the first 24 h of the oxic experiment are shown in the inset in A.

electron microscope operated at 200 kV with a Schottky field emitter as an electron source. The transmission electron microscope is equipped with a Gatan Imaging Filter (Tridiem) and a Fischione high-angle angular dark-field detector and an EDAX X-ray analyzer for simultaneous elemental analysis. Combined fast Fourier transform (FFT) was used to determine local structure and morphology of the secondary particles.

X-ray absorption near edge spectroscopy (XANES) combined with XRF mapping at beamline I14 of the Diamond Light Source (UK) was used on the oxic sample to determine the elemental distribution of Fe and Pb and to identify the speciation and oxidation states of Fe and Pb in the metal-binding phases. Python-based software ATHENA[36] and MANTIS were used for data processing. Complimentary extended X-ray absorption fine structure (EXAFS) spectra were collected at the ANKA-KIT synchrotron (Germany) SUL-X beamline to investigate the local bonding environment of Pb in both oxic and anoxic samples. Data reduction was performed using ARTEMIS software.[36] Details on the fitting procedures of XANES and EXAFS data are given in Supporting Information. Pure mineral model compounds were used to fit the XAS data; Pb(II)-adsorbed ferrihydrite was used as a representative for Pb(II) adsorption to ferric oxyhydroxide surfaces. The high carbonate solubility and reactivity of siderite impeded the preparation of Pb(II)-adsorbed siderite as a model.

The surface chemistry of the anoxic samples was investigated by XPS to determine Pb speciation on the siderite surfaces using a KRATOS Axis Ultra DLD. Data reduction was performed using UNIFIT software.[37]

2.4. Geochemical Modeling. Saturation indices of the phases involved in this study were calculated based on measured aqueous solution chemistry data using software PHREEQC[38] together with its 2017 Lawrence Livermore National Library database.

3. RESULTS

3.1. Pb(II) Uptake during Siderite Dissolution. In Pb(II)-bearing oxic aqueous solutions, the pH reached 4.5 within 2−3 h of reaction and continued to increase steadily to a final pH of 5.3 (Figure 1A). Simultaneously, Fe^{total} concentrations increased to 0.14×10^{-3} mol kg^{-1} during the first 2−4 h of reaction. A subsequent distinct drop in aqueous Fe^{total} concentrations and a visible change in the color of the suspension to reddish ochre indicated the precipitation of ferric (oxyhydr)oxides; the onset of ferrous iron oxidation and ferric oxyhydroxide precipitation may have initiated as soon as pH 4 was reached.[39] Within 2 h after the onset of siderite dissolution, 9 ± 3.6% of the initial aqueous Pb(II) was removed from the aqueous solution; after 1008 h, 90% of the Pb(II) was removed (Figure 1C). Under anoxic conditions, the pH of the Pb(II)-bearing aqueous solution increased to 5.1 within 0.5 h and to 6.5 after 96 h of reaction; from this time onward, the pH increased steadily to 6.9 at the end of the experiment (Figure 1B). The Fe^{total} concentrations peaked at 0.36×10^{-3} mol kg^{-1} after 168 h of reaction. Notably, Pb(II) was completely removed from the aqueous solution within 96−144 h of reaction (Figure 1D). The final aqueous Pb(II) concentrations were <10 μg L^{-1}, the upper limit of Pb(II) allowed in drinking water by the EU Council Directive,[40] which demonstrates the Pb(II) removal efficiency of this method.

3.2. Characterization of the Reaction Products. The solids recovered from the oxic and anoxic Pb(II)-bearing aqueous solutions after 1008 h were characterized using SEM imaging combined with EDX analyses, TEM, and XRD. An overview of the XRD results is given in Figure S3 and Table

S3. Measured *d*-spacings from TEM images and their corresponding FFT patterns are compiled in Table S4.

After 1008 h of reaction under oxic conditions, the recovered siderite grains were heterogeneously covered with secondary phases identified as nanoparticulate goethite (α-FeOOH) (Figure 2). Minor amounts of hematite (α-Fe_2O_3) were also present in the unreacted siderite starting material and are thus not considered a reaction product. The precipitates formed a discontinuous layer of $\leq$100−200 nm rods and needles randomly oriented to the siderite surface, partially radially intergrown, and occasionally intercalated with tabular crystallites (Figure 2A). Ultrafine precipitates collected from the reacted suspension consisted of *ca.* 5 nm long nanoparticles forming aggregates of $\leq$100 nm clumps with 100−200 nm long rods growing out of the clumps (Figure 2B). The lattice spacings in the clumped nanoparticles measured 2.25 Å (Figure 2C) and 2.56 Å in the rods (Figure 2D), identifying both precipitates as goethite. Faint spots in the FFT patterns (insets Figure 2C,D) from the particle aggregates exhibited lattice spacings of 2.40 and 2.79 Å, which suggest the presence of residual siderite, and of 3.87 Å, which suggests traces of hematite.

Siderite reacted with aqueous Pb(II) under anoxic conditions resulted in the precipitation of $\leq$5 μm rounded particles and micron-scale aggregates on the smooth but etched siderite surfaces (Figure 3A). EDX analyses of the reacted siderite grains, their surfaces, and the precipitates showed enrichment of Pb (Figures 3B and S4). XRD analyses identified nanocrystalline cerussite ($PbCO_3$) as the secondary phase (Figure S3). This was confirmed by TEM imaging and FFT analyses of the polycrystalline material attached to the siderite surfaces exhibiting *d*-spacings of 2.17, 2.63, and 2.92 Å, which are characteristic for cerussite (Figure 3C), while lattice spacings of 1.53 Å likely resulted from the presence of nearby siderite. No residual hematite from the unreacted material was found in the reacted solids, suggesting Fe(II)-induced reductive dissolution of this ferric component.[41−43] Notably, within the top 20 nm of a reacted siderite, a reaction zone was observed exhibiting a poorly (poly)crystalline phase oriented in a seemingly random angle to the underlying siderite. The lattice spacings of this phase matched those of the cerussite (Figure 3D,E).

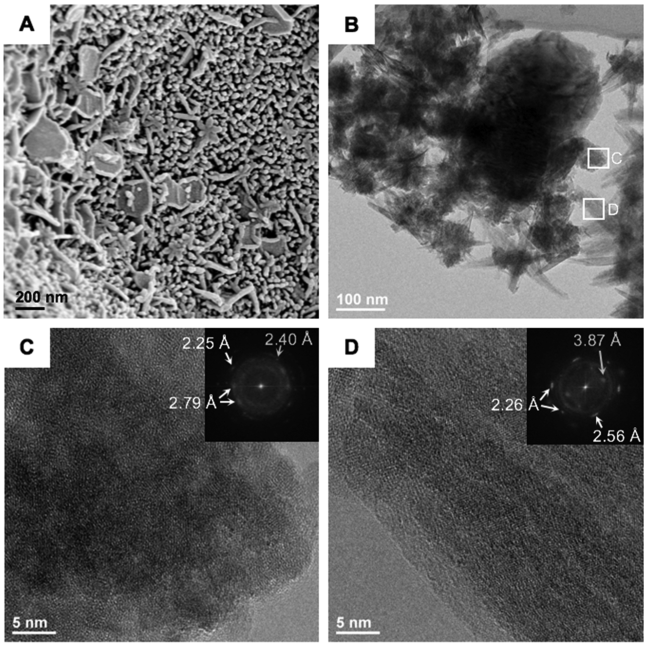

Figure 2. Scanning and transmission electron micrographs of siderite reacted in Pb(II)-bearing solutions for 1008 h under oxic conditions (Pb O LT). (A) Rod-shaped and intercalated pseudo-hexagonal tabular precipitates covering a siderite surface. (B) Ultrafine precipitates collected from the reactor suspension: a nearly completely reacted siderite fragment overgrown and surrounded by nanoparticulate precipitates forming clumps (C) and rods (D) *via* (nearly) oriented attachment; respective FFT patterns of the nanoparticles are indicative of goethite (2.25−2.26, 2.56 Å), traces of hematite (3.87 Å), and residual siderite (2.40, 2.79 Å). See Table S4 for measured *d*-spacings and reference data.

3.3. Speciation and Local Bonding Environment of Pb.

A set of complimentary XAS and XPS analyses were performed to determine the bonding environment of Pb associated with the solids recovered from the oxic and anoxic experiments. Results are presented in Figures 4, 5, and S5; respective fitting parameters are given in Tables 1, 2, and S5.

3.3.1. Pb Speciation and Bonding in the Oxic System.

Linear combination fitting (LCF) results of the Fe K-edge XANES spectra obtained from the bulk solid sample of the oxic experiment indicated that *ca.* 5% of the reacted solid-bound iron Fe(II) oxidized to Fe(III) during siderite dissolution in the presence of Pb(II) (Table 1). XRF elemental mapping of individual reacted siderite grains showed that Pb was present on all analyzed siderite surfaces; however, relatively higher concentrations were occasionally observed along the edges, while lower Pb concentrations were detected on (fracture) planes (Figure 4D−G). High-resolution XANES mapping of selected areas on grain surfaces showed that in areas of increased Pb concentrations, 83−85% of Fe was present as Fe(III). In areas with lower Pb concentrations, 79% of solid-bound Fe had remained as Fe(II) (Figure 4C). This Fe(II)−Fe(III) distribution on the reacted siderite surfaces indicates heterogeneous surface oxidation and/or covering with secondary ferric precipitates. Notably, LCF results of the Pb L_{III}-edge spectra of the same mapping area did not indicate a spatial correlation with or the preference of Pb for either iron oxidation state. In contrast, 39% of the solid-associated Pb was oxide-bound, and 61% was present as Pb carbonate (Figure 4F, area 1). In a mapped area of another grain of reacted siderite, the XRF element map indicated an equal distribution of Pb and a predominance of Fe(III) in the XANES map (Figure 4G, area 2). The LCF of the Pb L_{III}-near edge spectrum of this area, however, indicated a higher contribution of oxide-bound Pb over Pb carbonate (Figure 4B, area 2).

Shell-by-shell fits of the Pb L_{III}-edge EXAFS region of the solids indicate a first shell Pb−O interatomic distance R of R_{Pb-O} = 2.31 Å; this distance is indicative of Pb(II) adsorbed to iron (oxyhydr)oxides (Table 2). Previous studies reported radial distances of $R_{Pb-O} \leq 2.35$ Å for a distorted trigonal pyramidal coordination of Pb with the surface oxygen of goethite.[44−47] A second single scattering path of R_{Pb-Fe} = 3.31 Å falls within the reported range of R_{Pb-Fe} distances of 2.91−3.49 Å, indicative of the bidentate mononuclear inner-sphere surface complexation with FeO_6-octahedra in the iron (oxyhydr)oxide surface.[44] The coordination number of this pathway is similar (0.55) to values observed in previous EXAFS studies of Pb adsorbed on Fe(III) oxyhydroxide surfaces[20] and lies within the range of values expected for a bidentate mononuclear surface complex ($\leq$1.0). In contrast to

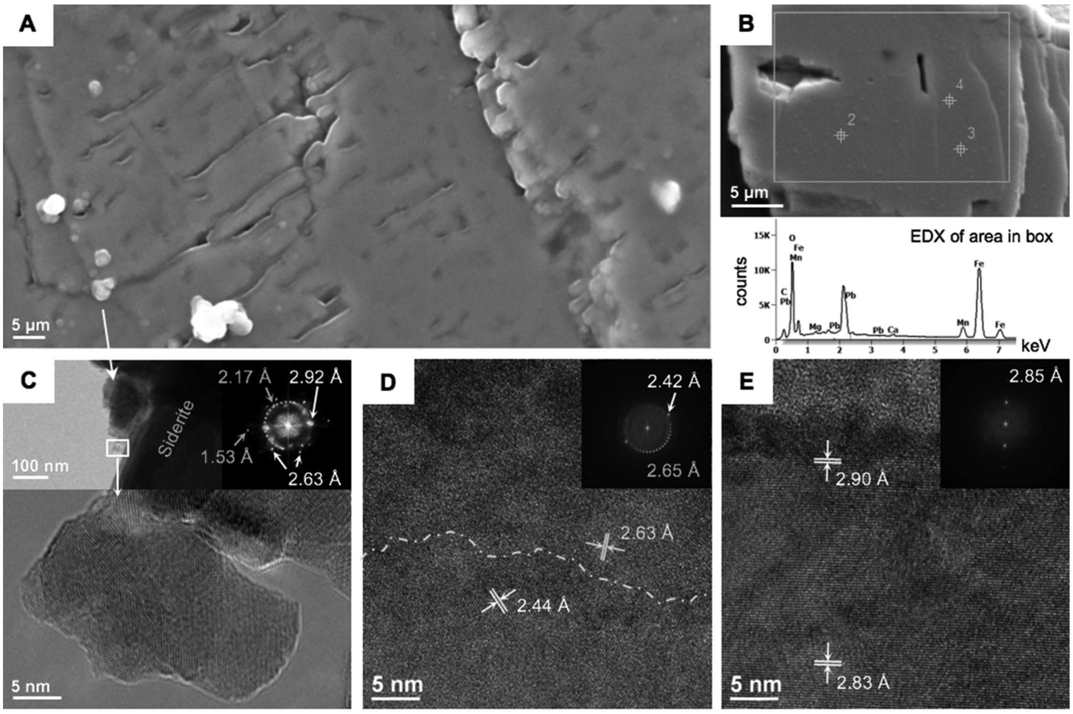

Figure 3. Scanning and transmission electron micrographs of siderite reacted in Pb(II)-bearing aqueous solutions for 1008 h under anoxic conditions (Pb A LT). (A) Reacted siderite grains showing dissolution-features, micron-scale precipitates, and Pb-enrichment on the surface (B). (C) TEM and the respective FFT pattern identify the precipitates as cerussite (2.63, 2.92 Å) attached to siderite (1.53, 2.17 Å). (D) Structurally independent cerussite (2.63−2.65 Å) growth on the reacted siderite surface (2.44 Å). (E) Widening of the siderite crystal lattice (2.83 Å) near the reacted surface to *d*-spacings indicative for cerussite (2.90 Å). See Table S4 for measured *d*-spacings and reference data.

the clear indication of Pb-carbonate environments in the XANES spectra, the EXAFS data lack unambiguous evidence of carbon scattering. Reasons for this may be a combination of methodologic limitations and sample specifics. Since carbon is a weak backscattering atom and lead is a strong absorber, the contribution of the Pb−C scattering with $R_{\text{Pb−C}} \geq 3.5$ Å to the EXAFS spectrum[20] may be insignificant in poorly crystalline materials such as the reacted siderite surface and Pb surface complexes.[48] The wide but discontinuous coverage of siderite grain surfaces with precipitates observed in SEM imaging and the continuous presence of Pb-carbonate species indicated in XANES mapping (Figure 4) suggest that Pb is also associated with carbonate at the siderite surface. It seems likely, therefore, that the observed contributions of Pb−C scatterings to the EXAFS spectrum of the bulk sample were overshadowed by the more prominent Pb−Fe scattering of Pb.

3.3.2. Pb Speciation and Bonding in the Anoxic System. XANES Fe K-edge spectra of the bulk solids collected from the anoxic experiments confirmed that Fe(II) oxidation did not occur, and all solid-bound Fe(II) remained as carbonate (Figure 4A). LCF of the respective Pb L_{III}-edge spectra indicates that 100 ± 3.6% of the solid-bound Pb(II) was present as carbonate (Table 1). In the EXAFS Pb L_{III}-edge shell fitting, the spectrum could be closely fit to cerussite with physically reasonable deviations from the ideal structure indicating that Pb is present in a 9-fold coordination[49] (Table 2).

Additional XPS analyses of the anoxic sample (Table S5) showed Pb $4f_{7/2}$ and $4f_{5/2}$ peaks at binding energies of 138.6 and 143.5 eV, respectively. These agree well with the binding energies reported for Pb(II) in Pb-carbonates,[50,51] Pb-calcite,[15] and Pb-aragonite[52] (Figure 5). Shifts toward higher binding energies by 0.3 and 0.4 eV observed in the O 1s and C 1s spectra of the reacted sample indicative for MeCO_3[53,54] suggest a change from the calcite-type into the aragonite-type carbonate structure.[52]

4. DISCUSSION

4.1. Reaction Mechanisms of Pb(II) Removal during Siderite Dissolution.

Siderite dissolves readily in acidic aqueous solution, with its solubility decreasing with increasing pH.[34,55] Its reaction products differ strongly under different redox conditions due to the redox sensitivity of the ferrous iron released into the reactive solution, which influences the mechanisms of Pb(II) removal from the reactive solution.

4.1.1. Siderite Dissolution-Coupled Iron Oxidation and Goethite Precipitation. During siderite dissolution under oxic conditions, the released ferrous iron oxidizes and precipitates as goethite nanoparticles after >2 h of reaction at a pH of ≥4.5 consistent with the reaction

$$\text{FeCO}_3(\text{s}) + 1/2\text{O}_2 + \text{H}_2\text{O} \rightarrow \alpha\text{-FeOOH}(\text{s}) + \text{HCO}_3^- \quad (1)$$

Note that the aqueous solution pH continuously increased during the experiment. This suggests that proton-consuming siderite dissolution dominates over proton-releasing reactions of iron oxidation, precipitation and adsorption during the oxic experiments. TEM and SEM imaging showed heterogeneously distributed precipitates, particularly growing along crystal edges, and nanorods growing from the siderite surface at random orientations. Similar observations were reported by Renard *et al.*,[56] showing interface-coupled siderite dissolution and structurally independent secondary ferric iron phase precipitation. Structurally independent discontinuous precip-

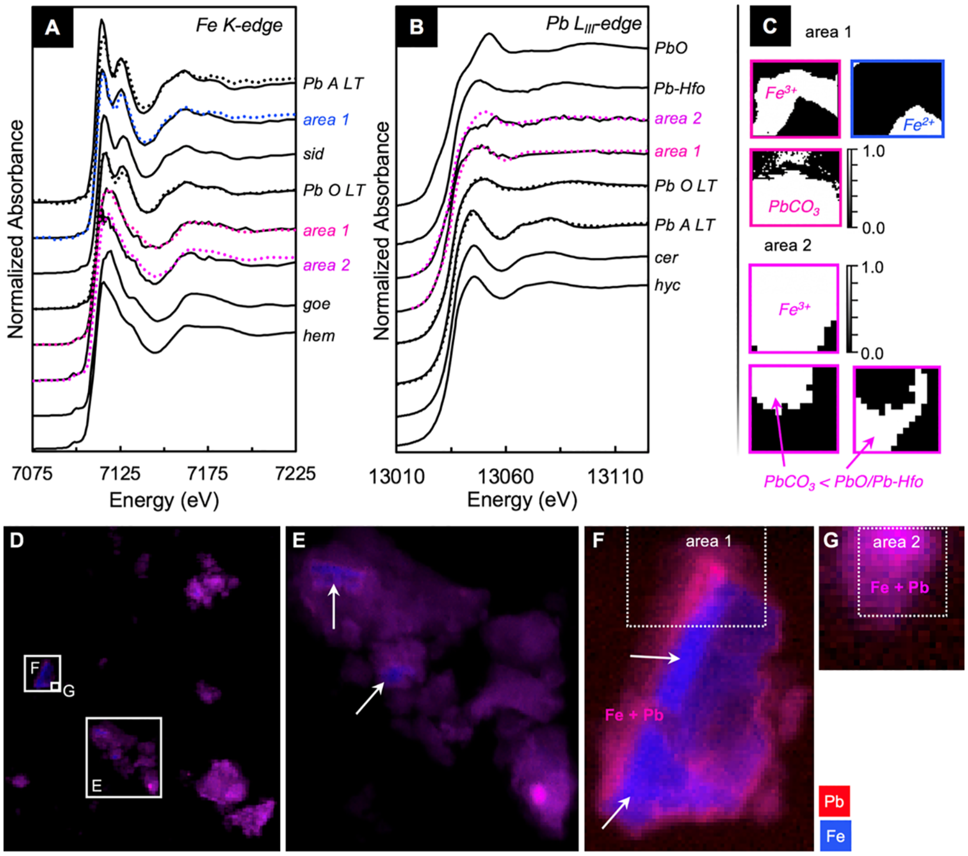

Figure 4. XANES spectra of model compounds and reacted siderite in the presence of aqueous Pb(II) under oxic and anoxic conditions after 1008 h of reaction. (A) Fe K-edge of samples and standards. (B) Pb L_{III}-edge of samples and standards. Pb A LT = anoxic long-term experiment and Pb O LT = oxic long-term experiment; sid = siderite, goe = goethite, hem = hematite, PbO = massicot (orthorhombic), Pb-Hfo = Pb-adsorbed hydrous ferric oxide (ferrihydrite), cer = cerussite, and hyc = hydrocerussite. Black lines represent bulk sample analyses. Dotted lines represent linear combination (LC) fits; colored lines correspond to high-resolution XANES mapping areas (C) in (F) (area 1; 6.5 × 5.5 μm) and (G) (area 2; 1.5 × 1.5 μm) mapped at a 100 × 100 nm pixel size. Note that in all XANES spectra are mixtures of Fe and Pb bonding environments (see Table 1); the dominant species are indicated in (C). (D−G) High-resolution XRF maps of reacted siderite grains reacted in Pb(II)-bearing aqueous solution under oxic conditions (Pb O LT); white outlines in (D) indicate magnified areas shown in (E−G). Red = Pb, blue = Fe, and magenta = Fe + Pb. Note that the Pb distribution varies only slightly and locally; strongly blue (Fe-rich) areas possibly indicate precipitate-free surfaces or fracture planes (white arrows). Image dimensions: (D) = 165 × 145 μm, (E) = 45 × 38 μm, (F) = 18 × 13 μm, and (G) = 2.5 × 2.5 μm.

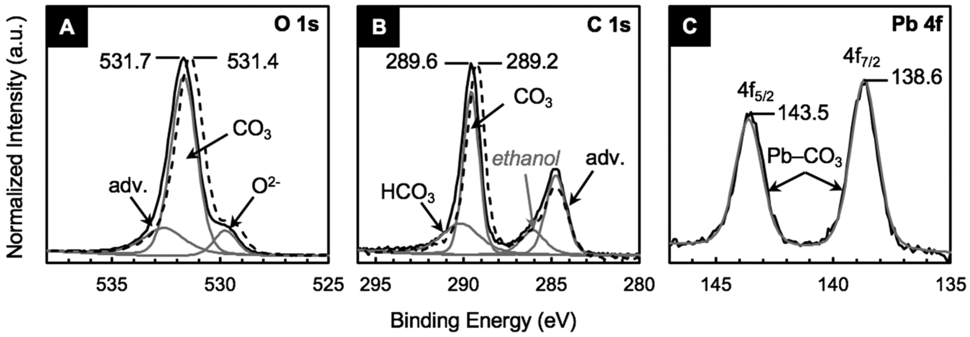

Figure 5. XPS spectra of the (A) O 1s, (B) C 1s, and (C) Pb 4f photoelectron lines obtained from the siderite sample reacted with aqueous Pb(II) for 1008 h under anoxic conditions (Pb A LT) shown as solid black curves; spectra obtained from the unreacted siderite sample are shown for comparison in dashed curves. Grey curves show the best fits of the spectra of the reacted sample. Adv. = adventitious carbon. Shifts in the O 1s and C 1s spectra of the reacted sample relative to the unreacted siderite samples toward higher energies by 0.3 and 0.4 eV, respectively, indicate a change in the carbonate structure, possibly due to recrystallization from siderite to cerussite on the reacted siderite surface.[52] The ethanol detected in the C 1s spectra originates from sample storage in ethanol.

itation suggests heterogeneous nucleation and growth on the siderite surface, arising from the structural dissimilarity between the dissolving trigonal parent material siderite and the orthorhombic goethite precipitate.[57] Such coatings contain pores allowing the reactive fluid to continuously dissolve the substrate without affecting the dissolution rate (Figure S6 and Table S6); a similar process has been suggested for otavite (Cd-carbonate) precipitation on aragonite.[58] There was no

Table 1. XANES Fe K-Edge and Pb L_{III}-Edge Linear Combination Fitting Parameters and Speciation of Solids Collected from Both Oxic[e] and Anoxic[f] Long-Term Experiments Measured in Bulk and at High Resolution Mapping[a]

Fe K-edge	sample	χ^2	χ^2_{reduced}	adsorbed	oxide	carbonate	
					Fe_2O_3 (Fe^{3+})	$FeCO_3$ (Fe^{2+})	error ± (%)
Pb O LT[e]	bulk	0.04	0.0006		4.9	95.1	3.1
	area 1[c]	0.93	0.0095		83.1	16.9	9.0
	area 1[c]	0.07	0.0013		20.8	79.2	4.5
	area 2[d]	0.04	0.0007		85.1	14.9	3.4
Pb A LT[f]	bulk	0.27	0.0040		–	100.00	0.0
Pb L_{III}-edge	sample	χ^2	χ^2_{reduced}	Pb-Hfo[g]	PbO	$PbCO_3$	error ± (%)
Pb O LT	bulk	0.01	0.0001	55.9[h]	25.4[g]	18.7	2.0
	area 1[c]	0.03	0.0008	–[h]	38.6	61.4	5.2
	area 2[d]	0.06	0.0012	19.0	54.4	26.6	1.8
Pb A LT	bulk	0.02	0.0001	–	–	100.0	3.6

[a] Area 1 measured 6.5 × 5.5 μm (Figure 4F), area 2 covered 1.5 × 1.5 μm (see Figure 4G). [b] Fit results normalized to 100%. [c] See Figure 4C,F. [d] See Figure 4C,G. [e] Oxic LT experiment; see Table S1 for experimental specifications. [f] Anoxic LT experiment; see Table S1 for experimental specifications. [g] Pb-Hfo = Pb-adsorbed hydrous ferric oxide (ferrihydrite). [h] Fits using only Pb-Hfo and no PbO resulted in poorer fit statistics.

Table 2. EXAFS Pb L_{III}-edge k^3-Weighed Shell Fitting Parameters and Interatomic Path Lengths Measured on Bulk Solid Samples from Both Oxic[d] and Anoxic[e] Long-Term Experiments[a,c]

	ΔE_0 (eV)	R-range (Å)	shell	N	R (Å)	σ^2 (Å^2)
Pb O LT[d]	−6.7 (2.1)	1.2−4.0	Pb−O	2.24 (0.18)	2.31 (0.03)	0.01[b]
			Pb−Fe	0.55 (0.25)	3.31 (0.02)	0.01[b]
Pb A LT[e]	−0.05 (3.5)	1.5−5.0	Pb−O	8.94 (2.91)	2.65 (−0.02)	0.027 (0.006)
			Pb−C	3[b]	3.15 (0.07)	0.027 (0.006)
			Pb−Pb	6[b]	4.15 (−0.07)	0.014 (0.004)

[a] Uncertainties are given in brackets. [b] Parameter was set during fitting. [c] ΔE_0 = energy shift. N = coordination number (degeneracy). R = interatomic path lengths. σ^2 = Debye−Waller disorder term. The amplitude reduction factor ($S_0{}^2$) was set to 0.9 in all fits. [d] Oxic LT experiment; see Table S1 for experimental specifications. [e] Anoxic LT experiment; see Table S1 for experimental specifications.

evidence for potentially dissolved atmospheric CO_2(g) enhancing siderite dissolution upon exposure to air during sampling. As the aqueous solution pH was less than 6, such effects would be insignificant.[59]

4.1.2. Coupled Siderite Dissolution and Cerussite Precipitation. Under both oxic and anoxic conditions, initial aqueous Pb(II) concentrations decreased with the onset of siderite dissolution. Under oxic conditions, *ca.* 9% of Pb(II) was removed from solution during the first 2 h of reaction, before the visible precipitation of goethite. Within the first 0.5 h of reaction under anoxic conditions, *ca.* 13% Pb(II) was removed from solution. Complementary PHREEQC calculations based on the measured aqueous solution composition indicate that both oxic and anoxic Pb(II)-bearing aqueous solutions were saturated with respect to cerussite within less than 0.5 h of reaction and thus shortly after the onset of siderite dissolution (Table S7). Since cerussite is markedly less soluble (log K_{sp} = −13.2)[60,61] than siderite (log K_{sp} = −10.9)[33] under the investigated experimental conditions, Pb(II) preferentially precipitated as cerussite as soon as sufficient aqueous carbonate was available from siderite dissolution regardless the redox condition of the reactive solution.

Under oxic conditions, early siderite dissolution-induced cerussite precipitation may explain the Pb-carbonate scattering contributions of up to *ca.* 19% in bulk and locally up to *ca.* 60% of the solid-bound Pb(II) in the XANES spectra. The tabular crystallites observed in SEM images growing from the siderite surface of the solids collected from the oxic experiments after 2−72 h of reaction and the pseudo-hexagonal tabular crystallites observed among the surface layer of goethite formed by the end of the experiment (Figure S7) resemble cerussite precipitates formed on aragonite surfaces reported by Godelitsas *et al.*[52] Similar crystallites were also observed in the solids recovered from the anoxic experiments but were absent, however, in the solids collected from the Pb(II)-free experiments (Figure S8). These observations confirm cerussite formation under both redox conditions despite the lack of evidence for cerussite in the XRD analysis of the oxic sample, in which the minor quantities of cerussite formed were most likely overshadowed by the secondary goethite in this sample.

Under anoxic conditions, XRD, XPS, and XANES analyses confirmed crystalline cerussite formation and that 100% of the Pb is bound as a carbonate at the end of the LT experiment. Our TEM data of the reacted siderite suggest local changes of its near-surface structure. A 20 nm thick surface reaction zone, exhibiting a widening of the siderite lattice and overgrowths of poorly (poly)crystalline material, was observed, with both features exhibiting lattice distances indicative of cerussite (Figure 3D,E). Pb(II) has an ionic radius of 1.19 Å in octahedral coordination and an ionic radius of 1.35 Å in the 9-fold coordination as in cerussite.[49,62] These Pb(II) radii are 53 and 75% larger than the radius of octahedrally coordinated Fe(II) in siderite (0.780 Å).[62,63] Incorporation of Pb(II) into the dissolution-induced vacated FeO_6 site in siderite would thus lead to distortion and a marked widening of the siderite lattice, despite possible relaxation of the siderite surface structure due to dissolution. Although the relatively large Pb(II) and Ba(II) ions have been reported to incorporate into the $^{[6]}$Ca(II) site in calcite,[64,65] dilation around potentially incorporated Pb(II) ions into the much smaller $^{[6]}$Fe(II) site in siderite is expected to be much more significant than that observed for the incorporation of Pb(II) and Ba(II) into the larger metal site of Ca(II) (1.0 Å)[62] in calcite.[64] EXAFS shell fitting, however, clearly indicates the 9-fold coordination of Pb(II) in cerussite. The shift toward higher binding energies in the O and C 1s spectra further imply non-isotype mineral replacement. Although studies of Pb(II) sorption to calcite at pH 8.3 reported no evidence of Pb incorporation or solid solution formation,[17] slight variations in the initial Pb(II) concentrations and pH conditions can lead to the (co)-precipitation of Pb-carbonates.[66,67] Similar studies of $CaCO_3$ interaction with Pb and transition metals at pH 2.8 to 7 showed dissolution-induced (co)precipitation of divalent metal carbonates.[52,58,68−72] While the replacement of orthorhombic aragonite by isotypic cerussite is fast and results in an epitaxial layer,[52,72] the replacement of trigonal siderite by orthorhombic cerussite requires a structural change. Solvent-mediated transformation of non-isostructural carbonates show random orientation of the precipitate relative to its host substrate,[69,71,72] similar to what was observed in TEM analyses (Figure 3D). Therefore, a coupled process of dissolution and reprecipitation-controlled transformation as shown by Yuan *et al.*[71] and Di Lorenzo *et al.*[72] for the structurally independent replacement of trigonal calcite by orthorhombic cerussite likely explains the observed changes in surface structure and mineral phase. This was likely facilitated by micropore generation due to the differences in structure, solubility, and molar volume between siderite and cerussite.[58,71,72]

4.1.3. Pb(II) Adsorption to Goethite and Siderite. Under oxic conditions, the continued precipitation of goethite over time led to a wide, discontinuous coverage of the siderite surfaces and to the growth of these precipitates in the reactive fluid suspension through aggregation (Figures 2A,B and S7). Shell-by-shell fitting of the Pb L_{III}-edge EXAFS spectra of the bulk solid reaction products indicated interatomic distances of R_{Pb-O} = 2.31 Å and R_{Pb-Fe} = 3.31 Å in the first and second coordination shell, respectively (Table 2). Both interatomic distances are in perfect agreement with distances reported for Pb-adsorbed to goethite[47] and characteristic for inner-sphere bidentate edge-sharing Pb(II)-adsorption to iron (oxyhydr)-oxides.[44−47] This conclusion is supported by the XANES spectra of the bulk sample and area 2 (Figure 4). LC fits indicate a distorted trigonal pyramidal coordination of Pb(II) with surface oxygens characteristic for Pb(II) adsorbed to ferric (oxyhydr)oxides.[44] Some of the scattering contributions also indicate a distorted tetragonal pyramidal coordination of Pb(II) as in PbO (orthorhombic),[73,74] which implies the presence of an additional oxygen atom in the distorted adsorption coordination sphere. This may be supported by the first shell Pb−O distance, which is slightly longer than for a trigonal sorption geometry (R_{Pb-O} ∼ 2.25−2.28 Å).[44,74] Contributions of these scatterings are particularly prominent in the locally resolved XANES mapping spectra and potentially result from dehydration and enclosure of Pb(II) ions during advanced aggregation and growth of the iron oxyhydroxide surface precipitates on the reacted siderite grains. The absence of second-neighbor oxygens and the low coordination number suggest that Pb(II) is adsorbed rather than incorporated.[47,74] Also, the absence of third shell scatterings excludes ternary absorption of carbonate;[20] in contrast, the first-shell sensitive XANES spectrum suggests the Pb-carbonate coordination of cerussite.

Since at least *ca.* 9% of the initial Pb(II) concentrations in the reactive aqueous solution was likely consumed by cerussite formation preceding goethite precipitation, the majority of remaining carbonate-bound Pb(II) was likely consumed by the growth of the cerussite precipitates to ≥100 nm large crystallites (Figures 2A and S7) until the reactive aqueous solution reached equilibrium with respect to cerussite after approximately 500−600 h of reaction and a pH of 5.0 (Figure 1; Table S7). However, the early sorption of Pb(II) to siderite, as reported to occur within 30 min under acidic pH conditions,[75] cannot be ruled out. Bivalent metal carbonates $MeCO_3$ (with Me = Ca, Fe, Mn) generally exhibit a high affinity to sorb heavy metals such as Zn(II), Cd(II), and Pb(II) to their surfaces.[15−17,53,66−68,75,76] For siderite, the pH of neutral surface charge (pH_{PZC}; point of zero charge) is 5.3 ± 0.1.[77] At pH < pH_{PZC}, carbonate mineral surfaces exposed to aqueous solution adsorb protons;[77] in the presence of dissolved divalent metals, these can compete with protons for the carbonate surface sites, contributing to the development of a more positive surface charge below the pH_{PZC}.[78] This suggests that Pb(II) could also have sorbed to siderite early in our experiments, forming $>CO_3Pb^+$ surface complexes and[77,78] preceding precipitation and growth of cerussite on the siderite surface. Therefore, Pb(II) uptake from the oxic system was likely three-fold: (I) potential sorption to siderite, (II) precipitation as cerussite, and (III) adsorption to goethite. As siderite surface coverage by goethite precipitates advanced over time and the siderite dissolution rate significantly decreases at a pH ≥ 5,[34] the adsorption to goethite likely dominated the drawdown of aqueous Pb(II) toward the end of these experiments.

4.2. Environmental Implications. In nature, the redox conditions of metal-contaminated sites may not be constant over time, potentially causing sorbed metals to be released.[14,21] Siderite, however, can effectively remove and sustainably retain toxic Pb(II) by precipitation in cerussite from acidic aqueous solutions at varying redox conditions, with no additional harm to the environment. Under either oxygenated or reduced conditions, Pb(II) uptake is governed by siderite dissolution, which is accompanied by rapid increase in pH to less acidic conditions. Initially, some Pb(II) rapidly precipitated as cerussite under either redox condition, followed by its simultaneous sorption onto oxidation-induced goethite nanoprecipitates under oxic conditions or further precipitation as cerussite under anoxic conditions.

Both mechanisms generate products that are stable under the investigated experimental and comparable natural conditions. Potentially, these dissolution-coupled mechanisms complementarily ensure Pb(II) retention in systems undergoing redox fluctuations, such as contaminated soils, floodplains, or stream sediments. For example, goethite as the reaction product of the oxic experiment is very insoluble under oxic conditions (log K_{sp} = −39.80).[79] If, however, redox conditions change from oxic to anoxic, reductive dissolution of goethite may occur.[23,41−43,80] As a result, the strong inner-sphere complexes of Pb(II) with the goethite surface may become unstable and susceptible to desorption.[11,18] Under reduced and acidic conditions, however, Pb(II) readily precipitates as sparingly soluble cerussite. Since the solubility product of cerussite is substantially lower than that of siderite, Pb(II) is much less susceptible to be liberated from cerussite. Redox sensitivity of carbonate-bound Pb(II) is also negligible compared to Fe(III) (oxyhydr)oxide-adsorbed Pb(II). Notably, when Pb(II) was completely consumed by $PbCO_3$ formation within 96−144 h of the anoxic experiment, no release of Pb(II) was observed over the remaining experiment duration of >850 h. This is because of the low solubility and high stability of cerussite over a wide range of pH conditions,[60,81] inhibiting Pb remobilization. In turn, the oxygenation of the $FeCO_3-Pb/PbCO_3-H_2O$ system would provoke goethite precipitation and Pb(II) adsorption to goethite. The observed aggregation of the nanoparticulate goethite may additionally promote Pb(II) retention in the oxic system.[82,83] Elevated $pCO_2(g)$ at above neutral pH, as often present in soil fluids or carbonate-rich surface waters, may enhance Pb(II) retention by enhanced siderite dissolution,[59] cerussite precipitation,[60,81] and/or ternary surface complexation on ferric (oxyhydr)oxide precipitates.[20]

5. CONCLUSIONS

Siderite dissolution effectively removes 90 and 100% of the initial 0.48×10^{-3} mol kg^{-1} Pb(II) from acidic oxic and anoxic aqueous solutions *via* three main pathways: neutralization, Pb carbonate formation, and adsorption. Under either redox condition, the liberation of carbonate during siderite dissolution leads to rapid increase in reactive fluid pH. Simultaneously, Pb(II) rapidly precipitates as $PbCO_3$, which was identified by XRD, TEM, and EXAFS as nanoparticulate cerussite. Additional XANES mapping and XPS analyses confirmed Pb-carbonate formation on the siderite surface, which particularly controls Pb(II) consumption under anoxic conditions and during early stages of the reaction under oxic conditions. EXAFS shell-by-shell fitting showed that Pb(II) also readily forms inner-sphere Pb(II) adsorption complexes with the oxidation-induced goethite nanoprecipitates under oxic conditions, which dominates Pb(II) uptake from the oxic aqueous solution at a later stage of the reaction.

Overall, the nanoparticulate and scarcely soluble reaction products remained stable, and no Pb was rereleased over the entire experiment duration of 1008 h. Reduced conditions, however, allow faster and more stable capture of Pb(II) than oxic conditions because of cerussite formation. We further showed that the presence of Pb(II) does not affect the dissolution rate of the microgranular natural siderite material, which remained governed by the reactive solution pH and its saturation state in the aqueous system. As a common iron ore (current market price $103.30/t),[84] the material costs for siderite used as a remediation reagent can be estimated assuming a reaction efficiency based on this study of 13.5 mg Pb sequestered per g siderite. Treatment of water contaminated with 100 mg L^{-1} aqueous Pb(II) using natural siderite would cost approximately $0.69 per ton contaminated water or $2.00/t if using synthetic siderite.[85] This study thus demonstrates that natural siderite dissolution is an effective, low-cost, and sustainable Pb(II) sequestration method for potential acidic wastewater remediation applications under either redox condition.

■ ASSOCIATED CONTENT

Supporting Information

The Supporting Information is available free of charge at https://pubs.acs.org/doi/10.1021/acsearthspacechem.0c00180.

Methodology, microscopic and spectroscopic results, and geochemical calculations (PDF)

Chemical solution data (XLSX)

■ AUTHOR INFORMATION

Corresponding Authors

Lisa C. Füllenbach − *Department of Earth Sciences, University College London, London WC1E 6BT, U.K.;* orcid.org/0000-0001-7690-8013; Email: l.fuellenbach@ucl.ac.uk

Eric H. Oelkers − *Department of Earth Sciences, University College London, London WC1E 6BT, U.K.; GET, CNRS UMR 5563, 14 Avenue Edouard Belin, 3400 Toulouse, France;* Email: e.oelkers@ucl.ac.uk

Authors

Jeffrey Paulo H. Perez − *GFZ German Research Center for Geosciences, Telegrafenberg, 14473 Potsdam, Germany;* orcid.org/0000-0002-0256-0576

Helen M. Freeman − *GFZ German Research Center for Geosciences, Telegrafenberg, 14473 Potsdam, Germany; School of Chemical and Process Engineering, University of Leeds, Leeds LS2 9JT, U.K.*

Andrew N. Thomas − *Department of Applied Geosciences, Karlsruhe Institute of Technology, 76131 Karlsruhe, Germany*

Sathish Mayanna − *GFZ German Research Center for Geosciences, Telegrafenberg, 14473 Potsdam, Germany; Carl Zeiss Microscopy GmbH, 73447 Oberkochen, Germany*

Julia E. Parker − *Diamond Light Source, Didcot OX11 0DE, U.K.*

Jörg Göttlicher − *Karlsruhe Institute of Technology, Institute for Photon Science and Synchrotron Radiation, 76344 Eggenstein-Leopoldshafen, Germany*

Ralph Steininger − *Karlsruhe Institute of Technology, Institute for Photon Science and Synchrotron Radiation, 76344 Eggenstein-Leopoldshafen, Germany*

Jörg Radnik − *Federal Institute for Material Testing and Research (BAM), Division 6.1, 12203 Berlin, Germany;* orcid.org/0000-0003-0302-6815

Liane G. Benning − *GFZ German Research Center for Geosciences, Telegrafenberg, 14473 Potsdam, Germany; Department of Earth Sciences, Freie Universität Berlin, 12249 Berlin, Germany*

Complete contact information is available at: https://pubs.acs.org/10.1021/acsearthspacechem.0c00180

Author Contributions

The manuscript was written through contributions of all authors. All authors have given approval to the final version of the manuscript.

Notes

The authors declare no competing financial interest.

■ ACKNOWLEDGMENTS

This work was funded by the European Union's Horizon 2020 Marie Skłodowska-Curie Innovative Training Network grant no. 675219. L.G. Benning acknowledges the financial support from the German Helmholtz Recruiting Initiative funding (award number I-044-16-01). Synchrotron mapping work was carried out with the support of the Diamond Light Source, instrument I14 (proposal MG21719-1). EXAFS work was conducted with the support of the ANKA-KIT, instrument SUL-X (proposal A2017-028-012253). Many thanks go to I. Wood for the XRD analyses, to G. Saldi for providing BET measurements, to A. Schreiber for preparing FIB sections for TEM, and to J. Stockmann (BAM) for performing the XPS measurements.

ABBREVIATIONS

Pb, lead; Pb O (LT), siderite dissolution experiment in Pb(II)-bearing solution under oxic conditions (long-term); Pb A (LT), siderite dissolution experiment in Pb(II)-bearing solution under anoxic conditions (long-term); ICP−OES, inductively coupled plasma optical emission spectroscopy; SFA, segmented flow analysis; XRD, X-ray (powder) diffraction; (FE-)SEM, (field emission) scanning electron microscopy; EDX, energy dispersive X-ray spectroscopy; FIB, focused ion beam; (HR)TEM, (high-resolution) transmission electron microscopy; XAS, X-ray absorption spectroscopy; XANES, X-ray absorption near edge structure; EXAFS, extended X-ray absorption fine structure; XRF, X-ray fluorescence; XPS, X-ray photoelectron spectroscopy

REFERENCES

(1) Lim, H.-S.; Lee, J.-S.; Chon, H.-T.; Sager, M. Heavy metal contamination and health risk assessment in the vicinity of the abandoned Songcheon Au−Ag mine in Korea. *J. Geochem. Explor.* **2008**, *96*, 223−230.

(2) Antoniadis, V.; Shaheen, S. M.; Boersch, J.; Frohne, T.; Du Laing, G.; Rinklebe, J. Bioavailability and risk assessment of potentially toxic elements in garden edible vegetables and soils around a highly contaminated former mining area in Germany. *J. Environ. Manage.* **2017**, *186*, 192−200.

(3) Kasassi, A.; Rakimbei, P.; Karagiannidis, A.; Zabaniotou, A.; Tsiouvaras, K.; Nastis, A.; Tzafeiropoulou, K. Soil contamination by heavy metals: Measurements from a closed unlined landfill. *Bioresour. Technol.* **2008**, *99*, 8578−8584.

(4) Sun, C.; Liu, J.; Wang, Y.; Sun, L.; Yu, H. Multivariate and geostatistical analyses of the spatial distribution and sources of heavy metals in agricultural soil in Dehui, Northeast China. *Chemosphere* **2013**, *92*, 517−523.

(5) Adamcová, D.; Radziemska, M.; Ridošková, A.; Bartoň, S.; Pelcová, P.; Elbl, J.; Kynický, J.; Brtnický, M.; Vaverková, M. D. Environmental assessment of the effects of a municipal landfill on the content and distribution of heavy metals in Tanacetum vulgare L. *Chemosphere* **2017**, *185*, 1011−1018.

(6) Wong, K. K.; Lee, C. K.; Low, K. S.; Haron, M. J. Removal of Cu and Pb from electroplating wastewater using tartaric acid modified rice husk. *Process Biochem.* **2003**, *39*, 437−445.

(7) Gäbler, H.-E.; Schneider, J. Assessment of heavy-metal contamination of floodplain soils due to mining and mineral processing in the Harz Mountains, Germany. *Environ. Geol.* **2000**, *39*, 774−782.

(8) Chen, Y.; Liu, Y.; Liu, Y.; Lin, A.; Kong, X.; Liu, D.; Li, X.; Zhang, Y.; Gao, Y.; Wang, D. Mapping of Cu and Pb contaminations in soil using combined geochemistry, topography, and remote sensing: A case study on the Le'an River floodplain, China. *Int. J. Environ. Res. Public Health* **2012**, *9*, 1874−1886.

(9) Pan, Y.; Li, H. Investigating heavy metal pollution in mining brownfield and its policy implications: A case study of the Bayan Obo Rare Earth Mine, Inner Mongolia, China. *Environ. Manage.* **2016**, *57*, 879−893.

(10) Bargar, J. R.; Towle, S. N.; Brown, G. E., Jr.; Parks, G. A. Outer-sphere Pb(II) adsorbed at specific sites on single crystal α-alumina. *Geochim. Cosmochim. Acta* **1996**, *60*, 3541−3547.

(11) Strawn, D. G.; Scheidegger, A. M.; Sparks, D. L. Kinetics and mechanisms of Pb(II) sorption and desorption at the aluminum oxide−water interface. *Environ. Sci. Technol.* **1998**, *32*, 2596−2601.

(12) Strawn, D. G.; Sparks, D. L. The use of XAFS to distinguish between inner- and outer-sphere lead adsorption complexes on montmorillonite. *J. Colloid Interface Sci.* **1999**, *216*, 257−269.

(13) Covelo, E. F.; Vega, F. A.; Andrade, M. L. Simultaneous sorption and desorption of Cd, Cr, Cu, Ni, Pb, and Zn in acid soils. I. Selectivity sequences. *J. Hazard. Mater.* **2007**, *147*, 852−861.

(14) Davranche, M.; Bollinger, J.-C. Heavy metals desorption from synthesized and natural iron and manganese oxyhydroxides: Effect of reductive conditions. *J. Colloid Interface Sci.* **2000**, *227*, 531−539.

(15) Fulghum, J. E.; Bryan, S. R.; Linton, R. W.; Bauer, C. F.; Griffis, D. P. Discrimination between adsorption and coprecipitation in aquatic particle standards by surface analysis techniques: Lead distributions in calcium carbonates. *Environ. Sci. Technol.* **1988**, *22*, 463−467.

(16) Rouff, A. A.; Reeder, R. J.; Fisher, N. S. Pb(II) sorption with calcite: A radiotracer study. *Aquat. Geochem.* **2002**, *8*, 203−228.

(17) Elzinga, E. J.; Rouff, A. A.; Reeder, R. J. The long-term fate of Cu^{2+}, Zn^{2+}, and Pb^{2+} adsorption complexes at the calcite surface: An X-ray absorption spectroscopy study. *Geochim. Cosmochim. Acta* **2006**, *70*, 2715−2725.

(18) Gunneriusson, L.; Lövgren, L.; Sjöberg, S. Complexation of Pb(II) at the goethite (α-FeOOH)/water interface: The influence of chloride. *Geochim. Cosmochim. Acta* **1994**, *58*, 4973−4983.

(19) Ostergren, J. D.; Bargar, J. R.; Brown, G. E., Jr.; Parks, G. A. Combined EXAFS and FTIR investigation of sulfate and carbonate effects on Pb(II) sorption to goethite (α-FeOOH). *J. Synchrotron Radiat.* **1999**, *6*, 645−647.

(20) Ostergren, J. D.; Trainor, T. P.; Bargar, J. R.; Brown, G. E., Jr.; Parks, G. A. Inorganic ligand effects on Pb(II) sorption to goethite (α-FeOOH). I. Carbonate. *J. Colloid Interface Sci.* **2000**, *225*, 466−482.

(21) Calmano, W.; Hong, J.; Förstner, U. Binding and mobilization of heavy metals in contaminated sediments affected by pH and redox potential. *Water Sci. Technol.* **1993**, *28*, 223−235.

(22) Jensen, D. L.; Boddum, J. K.; Tjell, J. C.; Christensen, T. H. The solubility of rhodochrosite ($MnCO_3$) and siderite ($FeCO_3$) in anaerobic aquatic environments. *Appl. Geochem.* **2002**, *17*, 503−511.

(23) Pedersen, H. D.; Postma, D.; Jakobsen, R. Release of arsenic associated with the reduction and transformation of iron oxides. *Geochim. Cosmochim. Acta* **2006**, *70*, 4116−4129.

(24) Nordstrom, D. K. Hydrogeochemical processes governing the origin, transport and fate of major and trace elements from mine wastes and mineralized rock to surface waters. *Appl. Geochem.* **2011**, *26*, 1777−1791.

(25) Shaheen, S. M.; Rinklebe, J. Sugar beet factory lime affects the mobilization of Cd, Co, Cr, Cu, Mo, Ni, Pb, and Zn under dynamic redox conditions in a contaminated floodplain soil. *J. Environ. Manage.* **2017**, *186*, 253−260.

(26) Skousen, J. G.; Ziemkiewicz, P. F.; McDonald, L. M. Acid mine drainage formation, control and treatment: Approaches and strategies. *Extr. Ind. Soc.* **2019**, *6*, 241−249.

(27) Erdem, M.; Gür, F.; Tümen, F. Cr(VI) reduction in aqueous solutions by siderite. *J. Hazard. Mater.* **2004**, *113*, 217−222.

(28) Tang, Y.; Martin, S. T. Siderite dissolution in the presence of chromate. *Geochim. Cosmochim. Acta* **2011**, *75*, 4951−4962.

(29) Bibi, I.; Niazi, N. K.; Choppala, G.; Burton, E. D. Chromium(VI) removal by siderite ($FeCO_3$) in anoxic aqueous solutions: An X-ray absorption spectroscopy investigation. *Sci. Total Environ.* **2018**, *640−641*, 1424−1431.

(30) Jönsson, J.; Sherman, D. M. Sorption of As(III) and As(V) to siderite, green rust (fugerite) and magnetite: Implications for arsenic release in anoxic groundwaters. *Chem. Geol.* **2008**, *255*, 173−181.

(31) Renard, F.; Putnis, C. V.; Montes-Hernandez, G.; King, H. E. Siderite dissolution coupled to iron oxyhydroxide precipitation in the presence of arsenic revealed by nanoscale imaging. *Chem. Geol.* **2017**, *449*, 123−134.

(32) Ha, J.; Zhao, X.; Yu, R.; Barkay, T.; Yee, N. Hg(II) reduction by siderite ($FeCO_3$). *Appl. Geochem.* **2017**, *78*, 211−218.

(33) Bénézeth, P.; Dandurand, J. L.; Harrichoury, J. C. Solubility product of siderite ($FeCO_3$) as a function of temperature (25−250 °C). *Chem. Geol.* **2009**, *265*, 3−12.

(34) Duckworth, O. W.; Martin, S. T. Dissolution rates and pit morphology of rhombohedral carbonate minerals. *Am. Mineral.* **2004**, *89*, 554−563.

(35) Stookey, L. L. Ferrozine—A new spectrophotometric reagent for iron. *Anal. Chem.* **1970**, *42*, 779−781.

(36) Ravel, B.; Newville, M. ATHENA, ARTEMIS, HEPHAESTUS: data analysis for X-ray absorption spectroscopy using IFEFFIT. *J. Synchrotron Radiat.* **2005**, *12*, 537−541.

(37) Hesse, R.; Bundesmann, C.; Denecke, R. Automatic spike correction using UNIFIT 2020. *Surf. Interface Anal.* **2019**, *51*, 1342−1350.

(38) Parkhurst, D. L.; Appelo, C. A. J. Description of input and examples for PHREEQC version 3−A computer program for speciation, batch-reaction, one-dimensional transport, and inverse geochemical calculations *U.S. Geological Survey Techniques and Methods, Book 6*; U.S. Geological Survey: Denver, Colorado, 2013; pp 1−497.

(39) Morgan, B.; Lahav, O. The effect of pH on the kinetics of spontaneous Fe(II) oxidation by O_2 in aqueous solution − basic principles and a simple heuristic description. *Chemosphere* **2007**, *68*, 2080−2084.

(40) European Union Council Directive 98/83/EC. *On the Quality of Water Intended for Human Consumption OJ L 330*. 1998L0083-EN-07.10.2015; Commission Directive (EU) 2015/1787; The Council of the European Union: Brussels, 2015; https://eur-lex.europa.eu/legal-content/EN/TXT/PDF/?uri=CELEX:01998L0083-20151027&from=EN.

(41) Wehrli, B.; Sulzberger, B.; Stumm, W. Redox processes catalyzed by hydrous oxide surfaces. *Chem. Geol.* **1989**, *78*, 167−179.

(42) Stumm, W.; Sulzberger, B. The cycling of iron in natural environments: Considerations based on laboratory studies of heterogeneous redox processes. *Geochim. Cosmochim. Acta* **1992**, *56*, 3233−3257.

(43) Pedersen, H. D.; Postma, D.; Jakobsen, R. Release of arsenic associated with the reduction and transformation of iron oxides. *Geochim. Cosmochim. Acta* **2006**, *70*, 4116−4129.

(44) Bargar, J. R.; Brown, G. E., Jr.; Parks, G. A. Surface complexation of Pb(II) at oxide−water interfaces: II. XAFS and bond-valence determination of mononuclear Pb(II) sorption products and surface functional groups on iron oxides. *Geochim. Cosmochim. Acta* **1997**, *61*, 2639−2652.

(45) Bargar, J. R.; Brown, G. E., Jr.; Parks, G. A. Surface complexation of Pb(II) at oxide-water interfaces: III. XAFS determination of Pb(II) and Pb(II)-chloro adsorption complexes on goethite and alumina. *Geochim. Cosmochim. Acta* **1998**, *62*, 193−207.

(46) Trivedi, P.; Dyer, J. A.; Sparks, D. L. Lead sorption onto ferrihydrite. 1. A Macroscopic and spectroscopic assessment. *Environ. Sci. Technol.* **2003**, *37*, 908−914.

(47) Liu, H.; Lu, X.; Li, M.; Zhang, L.; Pan, C.; Zhang, R.; Li, J.; Xiang, W. Structural incorporation of manganese into goethite and its enhancement of Pb(II) adsorption. *Environ. Sci. Technol.* **2018**, *52*, 4719−4727.

(48) Newville, M. Fundamentals of XAFS. *Rev. Mineral. Geochem.* **2014**, *78*, 33−74.

(49) Chevrier, G.; Giester, G.; Heger, G.; Jarosch, D.; Wildner, M.; Zemann, J. Neutron single-crystal refinement of cerussite, $PbCO_3$, and comparison with other aragonite-type carbonates. *Z. Kristallogr.* **1992**, *199*, 67−74.

(50) Pederson, L. R. Two-dimensional chemical state plot for lead using XPS. *J. Electron Spectrosc. Relat. Phenom.* **1982**, *28*, 203−209.

(51) Feng, Q.; Wen, S.; Zhao, W.; Deng, J.; Xian, Y. Adsorption of sulfide ions on the cerussite surfaces and implications for floatation. *Appl. Surf. Sci.* **2016**, *360*, 365−372.

(52) Godelitsas, A.; Astilleros, J. M.; Hallam, K.; Harissopoulos, S.; Putnis, A. Interaction of calcium carbonates with lead in aqueous solutions. *Environ. Sci. Technol.* **2003**, *37*, 3351−3360.

(53) Stipp, S. L.; Hochella, M. F., Jr. Structure and binding environments at the surface as observed with X-ray photoelectron spectroscopy (XPS) and low energy electron diffraction (LEED). *Geochim. Cosmochim. Acta* **1991**, *55*, 1723−1736.

(54) Duckworth, O. W.; Martin, S. T. Role of molecular oxygen in the dissolution of siderite and rhodochrosite. *Geochim. Cosmochim. Acta* **2004**, *68*, 607−621.

(55) Golubev, S. V.; Bénézeth, P.; Schott, J.; Dandurand, J. L.; Castillo, A. Siderite dissolution kinetics in acidic aqueous solutions from 25 to 100 °C and 0 to 50 atm pCO_2. *Chem. Geol.* **2009**, *265*, 13−19.

(56) Renard, F.; Røyne, A.; Putnis, C. V. Timescale of interface-coupled dissolution-precipitation reactions on carbonates. *Geosci. Front.* **2019**, *10*, 17−27.

(57) Kleber, W.; Bautsch, H.-J.; Bohm, J. *Einführung in die Kristallographie*, 19th ed.; Oldenbourg Verlag: München, 2010.

(58) Cubillas, P.; Köhler, S.; Prieto, M.; Causserand, C.; Oelkers, E. H. How do mineral coatings affect dissolution rates? An experimental study of coupled $CaCO_3$ dissolution−$CdCO_3$ precipitation. *Geochim. Cosmochim. Acta* **2005**, *69*, 5459−5476.

(59) Bruno, J.; Wersin, P.; Stumm, W. On the influence of carbonate in mineral dissolution: II. The solubility of $FeCO_3(s)$ at 25 °C and 1 atm total pressure. *Geochim. Cosmochim. Acta* **1992**, *56*, 1149−1155.

(60) Bilinski, H.; Schindler, P. Solubility and equilibrium constants of lead in carbonate solutions (25 °C, I = 0.3 mol dm^{-3}). *Geochim. Cosmochim. Acta* **1982**, *46*, 921−928.

(61) Grauer, R. *Solubility Products of M(II)-Carbonates*; PSI: Bericht No. 99-04. ISSN 1019-0643, 1999.

(62) Shannon, R. D. Revised effective ionic radii and systematic studies of interatomic distances in halides and chalcogenides. *Acta Crystallogr. A* **1976**, *32*, 751−767.

(63) Effenberger, H.; Mereiter, K.; Zemann, J. Crystal structure refinements of magnesite, calcite, rhodochrosite, siderite, smithsonite, and dolomite, with discussion of some aspects of the stereochemistry of calcite type carbonates. *Z. Kristallogr.* **1981**, *156*, 233−243.

(64) Reeder, R. J.; Lamble, G. M.; Northrup, P. A. XAFS study of the coordination and local relaxation around Co^{2+}, Zn^{2+}, Pb^{2+}, and Ba^{2+} trace elements in calcite. *Am. Mineral.* **1999**, *84*, 1048−1060.

(65) Callagon, E.; Fenter, P.; Nagy, K. L.; Sturchio, N. C. Incorporation of Pb at the calcite (104)−water interface. *Environ. Sci. Technol.* **2014**, *48*, 9263−9269.

(66) Rouff, A. A.; Elzinga, E. J.; Reeder, R. J.; Fisher, N. S. X-ray absorption spectroscopic evidence for the formation of Pb(II) inner-sphere adsorption complexes and precipitates at the calcite−water interface. *Environ. Sci. Technol.* **2004**, *38*, 1700−1707.

(67) Rouff, A. A.; Elzinga, E. J.; Reeder, R. J.; Fisher, N. S. The influence of pH on the kinetics, reversibility and mechanisms of Pb(II) sorption at the calcite−water interface. *Geochim. Cosmochim. Acta* **2005**, *69*, 5173−5186.

(68) Stipp, S. L.; Hochella, M. F., Jr.; Parks, G. A.; Leckie, J. O. Cd^{2+} uptake by calcite, solid-state diffusion, and the formation of solid-solution: Interface processes observed with near-surface sensitive techniques (XPS, LEED, and AES). *Geochim. Cosmochim. Acta* **1992**, *56*, 1941−1954.

(69) Prieto, M.; Cubillas, P.; Fernández-Gonzalez, Á. Uptake of dissolved Cd by biogenic and abiogenic aragonite: a comparison with sorption onto calcite. *Geochim. Cosmochim. Acta* **2003**, *67*, 3859−3869.

(70) Köhler, S. J.; Cubillas, P.; Rodríguez-Blanco, J. D.; Bauer, C.; Prieto, M. Removal of cadmium from wastewaters by aragonite shells and the influence of other divalent cations. *Environ. Sci. Technol.* **2007**, *41*, 112−118.

(71) Yuan, K.; Lee, S. S.; De Andrade, V.; Sturchio, N. C.; Fenter, P. Replacement of calcite ($CaCO_3$) by cerussite ($PbCO_3$). *Environ. Sci. Technol.* **2016**, *50*, 12984−12991.

(72) Di Lorenzo, F.; Cametti, G.; Vanhecke, D.; Churakov, S. V. The role of interfaces in controlling Pb^{2+} removal by calcium carbonate minerals. *Cryst. Growth Des.* **2020**, *20*, 6157−6169.

(73) Hill, R. J. Refinement of the structure of orthorhombic PbO (massicot) by rietveld analysis of neutron powder diffraction data. *Acta Crystallogr. C.* **1985**, *41*, 1281−1284.

(74) Bargar, J. R.; Brown, G. E., Jr.; Parks, G. A. Surface complexation of Pb(II) at oxide−water interfaces: I. XAFS and

bond-valence determination of mononuclear and polynuclear Pb(II) sorption products on aluminum oxides. *Geochim. Cosmochim. Acta* **1997**, *61*, 2617−2637.

(75) Erdem, M.; Özverdi, A. Lead adsorption from aqueous solution onto siderite. *Sep. Purif. Technol.* **2005**, *42*, 259−264.

(76) Zachara, J. M.; Kittrick, J. A.; Harsh, J. B. The mechanism of Zn^{2+} adsorption on calcite. *Geochim. Cosmochim. Acta* **1988**, *52*, 2281−2291.

(77) Charlet, L.; Wersin, P.; Stumm, W. Surface charge of $MnCO_3$ and $FeCO_3$. *Geochem. Cosmochim. Acta* **1990**, *54*, 2329−2336.

(78) Van Cappellen, P.; Charlet, L.; Stumm, W.; Wersin, P. A surface complexation model of the carbonate mineral-aqueous solution interface. *Geochim. Cosmochim. Acta* **1993**, *57*, 3505−3518.

(79) Hsu, P. H.; Marion, G. The Solubility Product of Goethite1. *Soil Sci.* **1985**, *140*, 344−351.

(80) Zinder, B.; Furrer, G.; Stumm, W. The coordination chemistry of weathering: II. Dissolution of Fe(III) oxides. *Geochim. Cosmochim. Acta* **1986**, *50*, 1861−1869.

(81) Taylor, P.; Lopata, V. J. Stability and solubility relationships between some solids in the system $PbO-CO_2-H_2O$. *Can. J. Chem.* **1984**, *62*, 395−402.

(82) Gilbert, B.; Ono, R. K.; Ching, K. A.; Kim, C. S. The effects of nanoparticle aggregation processes on aggregate structure and metal uptake. *J. Colloid Interface Sci.* **2009**, *339*, 285−295.

(83) Stegemeier, J. P.; Reinsch, B. C.; Lentini, C. J.; Dale, J. G.; Kim, C. S. Aggregation of nanoscale iron oxyhydroxides and corresponding effects on metal uptake, retention, and speciation: II. Temperature and time. *Geochim. Cosmochim. Acta* **2015**, *148*, 113−129.

(84) Tuck, C. C.; Phamdag, H. P. Mineral Industry Survey. Iron Ore in June 2020; USGS, September 2020. https://www.usgs.gov/centers/nmic/iron-ore-statistics-and-information.

(85) Guo, H.; Li, Y.; Zhao, K.; Ren, Y.; Wei, C. Removal of arsenite from water by synthetic siderite: Behaviors and mechanisms. *J. Hazard. Mater.* **2011**, *186*, 1847−1854.